Revised Manuscript (CLEAN - No tracked changes) Click here to view linked References

# Photocycle alteration and increased enzymatic activity in genetically modified photoactivable adenylate cyclase OaPAC

Katalin Raics[1], Katalin Pirisi [1], Bo Zhuang [2], Zsuzsanna Fekete[1], Nikolett Kis-Bicskei[1], Ildiko Pecsi [1], Kinga Pozsonyi Ujfalusi [1], Elek Telek [1], Yin Li[3], Jinnette Tolentino Collado [4], Peter J. Tonge [4], Stephen R. Meech[5], Marten H. Vos [2], Emoke Bodis [*1] and Andras Lukacs [*1]

[1]Department of Biophysics, Medical School, University of Pecs, Szigeti str. 12, 7624 Pecs, Hungary.

[2] Laboratoire d'Optique et Biosciences, Ecole Polytechnique, 91128 Palaiseau cedex, France

[3]Department of Physics, School of Physics and Materials Science, Nanchang University

[4]Department of Chemistry, Stony Brook University, New York, 11794, United States.

[5]School of Chemistry, University of East Anglia, Norwich, NR4 7TJ, U.K.

[*] Correspondence: andras.lukacs@aok.pte.hu; emoke.bodis@aok.pte.hu

## Abstract

Photoactivable adenylate cyclases (PAC) are light activated enzymes that combine blue light sensing capacity with the ability to convert adenosine triphosphate (ATP) to cyclic adenosine monophosphate (cAMP) and pyrophosphate (PPi) in a light-dependent manner. In most of the known PACs blue light regulation is provided by a BLUF domain which undergoes a structural reorganization after blue-light absorption. This minor structural change then is translated towards the C-terminal of the protein, inducing a larger conformational change that results in the ATP conversion to cAMP. As cAMP is a key second messenger in numerous signal transduction pathways regulating various cellular functions, photoactivable adenylate cyclases are of great interest in optogenetic studies. The optimal optogenetic device must be "silent" in the dark and highly responsive upon light illumination. OaPAC is a very good candidate as its basal activity is very small in the dark and the conversion rates increase 20-fold upon light illumination. We studied the effect of replacing D67 to N, in the BLUF domain. This mutation was found to accelerate the primary electron transfer process in the photosensing domain of the protein, as has been predicted. Furthermore, it resulted in a longer lived signalling state, which was formed with a lower quantum yield. Our studies show that the overall effects of the D67N mutation lead to a slightly higher conversion of ATP to cAMP, which points in the direction

that by fine tuning the kinetic properties more responsive PACs and optogenetic devices can be generated.

## Introduction

The photoactivated adenylate cyclase (PAC) from the cyanobacterium *Oscillatoria acuminata* (OaPAC) is a recently discovered flavoprotein that translates a blue-light signal into the production of cAMP(1). OaPAC is a homodimer of a 366-aa protein comprising an N-terminal BLUF (blue-light using FAD) domain and a C-terminal class III adenylyl cyclase (AC) domain. The AC activity of OaPAC is stimulated by light up to 20-fold above basal levels in the dark(1). Blue-light regulation of the majority of the PAC proteins is achieved by a BLUF domain. BLUF domains act as light sensing modules and are involved in a large range of light-controlled biological processes like bacteriochlorophyll biosynthesis, biofilm formation, phototaxis and controlling levels of cyclic-AMP.(2-8) Despite the diversity in the function of BLUF domains, the photosensing mechanism is similar: blue-light absorption by the flavin adenine dinucleotide (FAD) chromophore leads to a rearrangement of the hydrogen bonding network, which is reflected in a red-shift of ~ 10 nm of the $S_0$-$S_1$ flavin transition(8)**.**

The photoinduced mechanism of the BLUF domain is driven by the photochemistry of FAD: after blue light excitation, the flavin attracts an electron from the neighbouring electron-rich amino acids like tryptophans or tyrosines.(9-11) After the electron transfer step, either the anionic ($FAD^{\bullet-}$) or the neutral ($FADH^{\bullet}$) flavin radical is formed depending on the flavin environment. A similar process is crucial in the function of cryptochromes, where excitation of the oxidized flavin leads to electron transfer from the neighbouring tryptophan, forming the anionic flavin radical followed by protonation (on the microsecond timescale) to yield a semiquinone flavin radical form.(12-16) However, the actual role of electron transfer in BLUF domain proteins is still under debate, as it was not observed in AppA(17), BlsA(18), or BlrB(7), but was found to be crucial in PixD(5, 19) and PapB(20).

In the OaPAC BLUF domain (Fig. 1) a concerted proton coupled electron transfer process (PCET) takes place: upon excitation of FAD an electron is transferred from a nearby tyrosine (Y6) to the flavin while simultaneously a proton is transferred from Y6 to the adjacent glutamine (Q48) and later to the flavin. Aside the involvement in the PCET process Q48 plays a central role in the photoactivation and the function of the protein as it is thought to tautomerize

after the light excitation of flavin. Tautomerization of the glutamine was first proposed for AppA (21-28) but later was proven to be present in PixD (29-31) as well. Based on these findings it is a plausible assumption that during the PCET process Q48 tautomerizes, and this step is expected to be crucial in transmitting the signal to the C-terminal part of the protein where ATP is converted to cAMP. The role of Q48 should be further studied as it is expected to play a central role in the photoactivation and the overall function of OaPAC.

PACs are important for applications in the life sciences as the light-controlled cAMP production is a promising optogenetic tool: EuPAC was expressed in the neurons of the marine gastropod *Aplysia* enabling photocontrol of neuron stimulation(32), and bPAC was utilized in transgenic mice in light controlled flagellar beat of sperms(33). The latter has a 300-fold increase in cAMP conversion activity compared to OaPAC which has around a 20-fold activity increase(1, 34). It is therefore important to enhance control of the cyclase activity of OaPAC. In this work we investigated the functional dynamics of D67N mutant OaPAC, which shows an ~ 1.5-fold increase in light-induced AC activity of OaPAC as well as an acceleration of the forward and backward electron transfer processes and a decrease of the dark state recovery rate in the BLUF domain. The mutation slightly elevated the activity of the enzyme in the dark-adapted state as well, which points to a structural change extending to the enzymatic domain.

## Results and discussion

### Transient absorption measurements

Previously, ultrafast transient infrared and visible absorption spectroscopy were employed to investigate the photochemistry of OaPAC and it was established that after absorption of blue light by the flavin, a proton coupled electron transfer takes place(35). During the PCET process, the primary electron donor is the conserved Y6 tyrosine (35). Photoexcitation of the flavin leads to the extraction of an electron from the tyrosine accompanied by the transfer of a proton from the same tyrosine resulting in the formation of neutral (36)tyrosine and flavin radicals. In our previous work, we demonstrated that the AC activity of OaPAC is linked to this PCET process: as the $pK_a$ of the crucial tyrosine (Y6) was lowered from 9.9 to < 7.7, the photocycle was halted at $FAD^{\bullet-}$ and no enzymatic activity was observed(35).

Adiabatic quantum mechanical/molecular mechanical simulations performed on Slr1694 (also called PixD), another intensively studied(5, 19, 37) BLUF domain protein, suggested that the replacement of the negatively charged aspartic acid D69 (D67 in OaPAC, see Fig. 1) with a neutral or a positively charged residue will dramatically affect the electron transfer process(38). It was predicted that may demonstrate vastly different photocycle kinetics(38). Thus, here we investigate experimentally the potential effect of an analogous mutation on the photoactivation mechanism of OaPAC and measure the resulting enzymatic activity of the AC domain.

The primary photochemistry of the D67N mutant was characterised using transient absorption measurements. Ultrafast transient absorption (TA) spectroscopy is a powerful method to characterize the electron transfer processes in flavoproteins(4, 5, 7, 10, 14, 39-43). Depending on the protein environment the flavin chromophore can exist in five different redox states(44), and these redox states possess distinct absorption spectra (Fig. S1 A). Using these spectra one can perform spectral modelling in order to identify the flavin and amino acid radical species detected at different time delays after excitation.(10, 14, 45, 46)

The TA spectra of D67N OaPAC measured at early time delays (**Fig. 2A**) are similar to those of other (oxidized) flavoproteins**(10, 22)**, including WT OaPAC(35): an intense negative peak (bleach) is observed around 450 nm, which reflects disappearance of the S0 –> S1 absorption of the flavin. The positive peak around 510 nm is attributed to the absorption of the excited state, whereas the negative broad peak ~ 550 nm observed at the early time delays can be assigned to the stimulated emission of the flavin. The TA data for the WT protein could be globally fitted with three different time constants**(35)**, 5 ps, 83 ps and an infinite value (also called final state). Analysis of the corresponding EAS indicated that the 5-ps component reflects FAD* decay. The 83-ps components reflects decay of both FAD* and formation of $FADH^{\bullet}$. The FAD* decay kinetics, by electron and proton transfer to the flavin, are thus dispersive (see fluorescence kinetics below) and the slower phases cannot be kinetically disentangled from that of the formation and decay of the $FADH^{\bullet}$ intermediate state. The final state represents the red-shifted FADox signalling state. Similarly to the WT measurements, the TA data of D67N was also globally fitted with three different time constants (**Fig.2B**) of 5 ps, 65 ps, and infinite. The 5-ps EAS ascribed to FAD* decay resembles the 5 ps EAS of WT and EAS2 (65 ps phase for D67N) was equally modelled as a combination of the spectra of the excited flavin and the neutral flavin radical (see Fig. S1 B). The 5ps component thus reflects the formation of the neutral flavin radical and the 65 ps component the relaxation of the radical state (see Fig. S6). Yet, the relative contribution of FAD* to EAS2 appears smaller for D67N (~ 75 % in WT and

~ 60% in D67N), indicating also dispersive but faster overall FAD* decay (see also below). In addition, the second time constant is somewhat shorter in the mutant (65 ps vs. 85 ps) which also suggests a faster recombination of the radical pair. In WT OaPAC(35) the ~ 510 nm peak shifts towards 480 nm in ~80 ps; this shift is due to the formation of the signalling state. A similar shift is observed in D67N OaPAC mutant, but the amplitude of the final state EAS is smaller in the mutant compared to WT (see Fig. S5). Along with the finding that the spectrum of the signalling state is similar in WT and D67N OaPAC (see Fig. 5A below), this indicates lower quantum yield of formation of the signalling state. Based on the amplitude ratios of the final state- and the initially formed FAD* difference spectra (EAS final and 5-ps in Fig. S5) we estimate that the signalling state QY is ~4-fold lower in D67N than in WT OaPAC.

Observing the kinetics of the excited state absorption peak of the flavin (~ 505 nm) the mutant's relaxation appears sligtly faster compared to WT (**Fig. 2C);** applying a monoexponential fit the time constants for the WT and D67N were 90 ± 30 ps and 64 ± 8 ps respectively. This is due to faster FAD* decay kinetics (see below) as well as to the lower asymptotic value at this wavelength due to lower signalling state formation. The faster FAD* decay is in good agreement with the theoretical expectation that the replacement of the aspartic acid with a neutral or even positively charged amino acid will accelerate the electron transfer process as it alters the active site potential(38).

**Ultrafast Transient Fluorescence spectroscopy experiments**

To gain further information on the impact of D67N on the electron transfer process in OaPAC, we performed ultrafast transient fluorescence measurements on our home-built Kerr-gated fluorescence setup(47). The advantage of using the Kerr-gate approach compared to fluorescence upconversion is that the fluorescence emission spectrum can be obtained at every time delay whereas in the fluorescence upconversion method the decay of the fluorescent intensity is measured at one certain wavelength. **Fig. 3A)** and **3B)** show the EAS spectra obtained from the global fitting of the transient fluorescence dataset. The maximum of the fluorescence emission is at ~ 513 nm, which is slightly higher than that observed in AppA BLUF(48) (~ 500 nm) and significantly lower than of the free flavin (~ 530 nm). The fluorescence emission spectrum indicates that the flavin is embedded in a non-surface exposed environment. There is no significant difference between the emission maxima of WT and

mutant OaPAC, suggesting that the mutation did not result in significant change of the flavin environment.

The fluorescence of WT OaPAC, which was not reported before, was found to be highly dispersive as was observed in the case of AppA(6). The transient fluorescence dataset could be well described with the same three lifetimes (5 ps, 83 ps and infinite) as retrieved in the TA experiments. The corresponding EAS (species-associated spectra assuming a sequential scheme (1→2→3)) all peaked at ~ 513 nm, implying that they arise from protein-bound flavin, as the fluorescence emission maximum of free flavin is ~ 530 nm.

A global fit also resolved three components for the D67N mutant (5 ps, 60 ps, infinite, **Fig. 3B**), again with a shorter second time constants compared to the WT protein. The kinetic traces observed at 513 nm were overlaid (**Fig. 3C**) to compare the decay of the fluorescence emission of WT and D67N. The time constant of the excited state relaxation in D67N is almost half compared to that observed in the WT protein. This assessment, which is not complicated by contributions of product states as in TA experiments, unambiguously demonstrates that overall electron transfer is faster in D67N OaPAC mutant. Yet, as shown above, this modestly faster initial ET does not lead to a higher yield of the signalling state, presumably due to strongly enhanced back PCET from $FADH^{\bullet}$ to the resting dark state (49).

It is worth mentioning that the aspartate to asparagine mutation was suggested for PixD where the authors expected that the mutation would enhance significantly the electron transfer kinetics(38). We performed this homologous mutation in PixD (D69N) and it also resulted in faster fluorescence decay and shorter time constants (see Fig S2, S3). We also performed transient absorption measurements on PixD WT and D69N and we observed a similar shortening of the time constant of EAS2 (Fig. S4).

**Indirect measurement of cAMP**

An enzymatic assay was employed to examine the impact of accelerating the electron transfer process in the D67N mutant blue light sensing domain on the ability of the AC domain to convert ATP to cAMP plus pyrophosphate. The adenylate cyclase activities of 1 μM of WT OaPAC and D67N OaPAC were monitored using a spectrophotometric assay that detects pyrophosphate released by OaPAC when it converts ATP to cAMP. The inorganic pyrophosphatase enzyme converts pyrophosphate into two equivalents of phosphate which is then consumed by the MESG/PNP reaction and detected by an increase in absorbance at 360nm. **Fig.4A** shows the dark and the light-induced enzymatic activity of WT OaPAC and D67N

mutant OaPAC in the presence of 500 µM ATP. In the dark the enzymatic activity of the mutant is slightly higher compared to WT but still very low. Upon illumination the conversion rates strongly increased for WT and the D67N mutant. However D67N mutant converts ATP at a higher rate than WT making this mutant a starting point for tuning PACs as optogenetic tool. The enzymatic assays were performed using increasing amount of substrate and the results were evaluated using the classical Michelis-Menten presentation (see Fig 4B). The enzymatic essays show an elevated cAMP production in D67N OaPAC: the maximal velocity of the conversion rate was ~ 1.5 times higher in the mutant (0.100 ±0.002 mM/min) than in WT (0.064 ± 0.007 mM/min). The concentration of half-maximal velocity ($K_M$) is also slightly higher in the mutant than in WT, but more importantly the catalytic constant ($k_{cat}$) – which gives the number of substrate molecule each enzyme site can convert to product per unit time is ~ 1.5 times higher in D67N (50.05 1/min) than the WT OaPAC (32.2 1/min) (see Table 1).

**Recovery experiments**

The electronic spectrum of the mutant shows the typical red shift of the $S_0$-$S_1$ absorption peak (from 442 nm to 455 nm) after blue light irradiation, resembling WT OaPAC and other BLUF domain proteins (**Fig.5A**). We measured the dark state recovery of WT and D67N OaPAC to connect the photochemistry of the BLUF domain with the functional dynamics of the AC domain. Light to dark recovery of BLUF domains spans from dozens of minutes to a few seconds. In AppA the photocycle is relatively long, with a recovery lifetime of ~ 25 min(50), in PixD it is substantially shorter (~ 26 s) (8, 19) and in OaPAC it is only a couple of seconds(35). The dark state recovery of D67N mutant and WT OaPAC were monitored at 490 nm and the recovery rate of the mutant is ~ 5 times lower (15.3 s) than the recovery rate of WT OaPAC (3.6s) (**Fig.5B**). This significant change points to a possible structural difference between the mutant and the native protein. The slower recovery of D67N implies that after light excitation the protein spends more time in a structure allowing high-rate cAMP conversion. Altogether, the mutant adopts a structure that is not only more favourable for ATP to cAMP conversion but also slows down the rearrangement to the original structure.

**Differential Scanning Calorimetry (DSC) measurements**

The difference in the enzymatic activity and the dark state recovery suggests that the introduced mutation has changed the overall protein structure. To test this hypothesis, we performed differential scanning calorimetry (DSC) experiments on both proteins to examine their thermostability. These measurements reveal a significant difference between mutant and WT OaPAC. The thermal denaturation of WT showed a steep endothermic unfolding with a Tm of 68.1°C and a ΔH of 0.078 J/g. The measurement of D67N resulted in a lower Tm (62.1°C) with a lower ΔH (0.069 J/g). The melting temperature (Tm) is where 50% of the protein is denatured, while the area under the curve reflects the required energy for protein unfolding associated with the enthalpy change (ΔH). The smaller ΔH of D67N indicates a less compact conformation of the D67N mutant. This is also reflected by the considerably (6°C) lower Tm value (**Fig. 6**). This observation suggests that this structural change is at the origin of the elevated activity of D67N OaPAC.

**Fluorescence anisotropy-based nucleotide-binding assays**

It is not known what the affinity of ATP is in the dark- or light-adapted state of the protein. Therefore, using fluorescence anisotropy-based nucleotide-binding assays we measured the binding affinity ($K_D$) of a fluorescently labelled ATP analogue (MANT ATP) for the WT and D67N mutant. Fluorescence anisotropy provides a sensitive tool to measure the binding of ligands to proteins when a fluorophore is attached to the ligand(36). Changes in the anisotropy are caused by changes in the mobility of the fluorophore. The addition of OaPAC protein or mutant to MANT-ATP increases the fluorescence anisotropy of the N-Methylanthraniloyl (the labelled part of MANT-ATP) as binding of MANT-ATP to OaPAC results in an increase in the volume of the labelled entity and hence slows down its rotational movement. MANT-ATP was excited at $\lambda_{exc}$=350nm and the fluorescence anisotropy was detected at 450nm with increasing concentrations of OaPAC. It should be noted that the flavin in OaPAC emits > 500 nm and therefore there is no contribution from the flavin emission in the anisotropy measurements. The affinity ($K_D$) for MANT-ATP was determined to be 2.2 ± 0.4 mM for WT and 7.7 ± 1.6 mM for the mutant (**Fig.7**). The lower affinity found in the case of the mutant generally aligns with the conclusion that the mutation induces a structural change – as observed in the DSC measurements – which affected the binding affinity of ATP as well as the yield of the cAMP production.

## Concluding remarks

The D67N mutant, which was predicted to change the photocycle kinetics, was made in OaPAC. Based on the crystal structure of OaPAC, D67 is in hydrogen bonding distance to R79 (~3 Å) residue and to the ribityl chain (~3.2 Å) of flavin. D67 is a hydrogen bond acceptor and mutating D67 to N, a neutral amino acid, modulates the electrostatic potential of flavin by altering the hydrogen boding network. According to Goings et al.(38) the electrostatic potential at the center of flavin can be modulated by either moving positive charge toward the ring or moving negative charge away from the ring. In PixD, the Asp69−Arg71 pair is a good example of residues hydrogen bond to each other that have opposite effects on the active site potential. According to the QM/MM study done Goings et al.(38), when the Asp69−Arg71 pair moves closer to the flavin ring, the negatively charged Asp69 destabilizes charge transfer, whereas the positively charged Arg71 stabilizes charge transfer, and vice versa. When D67 is mutated to N the hydrogen bond length between the side chain of N67 and the ribityl chain of flavin is expected to increase, potentially favouring charge transfer.

Our ultrafast transient fluorescence measurements demonstrated that the overall kinetics of forward electron transfer was significantly faster in the mutant compared to WT, in qualitative agreement with the predictions of Goings et al(38). The transient absorption measurements also demonstrated ~4-fold weaker signalling state quantum yield, reflecting a much stronger acceleration of the back reaction competing with formation of the signalling state due to the mutation. A third kinetic effect of the mutation is the ~5-fold deceleration of the recovery of the dark state. Overall, these counterbalancing effects lead to ~similar acceleration of the enzymatic rate in WT and D67N OaPAC. However, as the basal activity of D67N OaPAC is somewhat higher than that of WT, the maximal enzymatic velocity $k_{cat}$ in the light state is ~ 1.5 higher in the mutant than in WT. This makes this mutant a better potential optogenetic tool as the basal activities are still low but the light-activated cAMP production is higher than in the native protein.

Upon excitation, the D67N mutant spends longer in the structure favouring the ATP to cAMP conversion. This suggests that the enzymatic activity is increased as the protein spends more in the signalling state despite its lower quantum yield. Our calorimetry

measurements showed that the melting temperature is considerably lower than observed in WT, indicating that the D67N mutant unfolds more easily. Hence, the mutant protein seems to possess a less compact structure than WT. The binding experiments also pointed to an altered enzymatic domain structure as WT OaPAC binds ATP slightly more strongly than the mutant.

Overall, future studies aiming at further tuning the relevant kinetic rates may provide a good road to increase the enzymatic activity of PACs

## Experimental Procedures

*Expression and purification of full-length wild type and D76N mutant OaPAC*

The D67N mutation was generated with Q5 Site-Directed Mutagenesis Kit (NEB) using WT full OaPAC/pCold-I as a template. The mutated construct was verified by DNA sequencing. The full WT or D67N OaPAC/pCold-I construct was transformed into *Escherchia coli* BL21(DE3) cells and grown on an LB-agar plate containing 100 µg/mL ampicillin. A single colony was used to inoculate 10 mL 2x-YT medium (Fisher Bioreagents, BP9743-5) containing 100 µg/mL ampicillin that was shaken overnight at 37°C (250 RPM). The 10 mL culture was used to inoculate 1 L of 2x-YT medium. The culture was shaken at 37 °C (250 RPM) until the OD600 reached ~0.8. The temperature was lowered to 18°C, and following 30 min incubation the protein expression was induced by adding 1 mM IPTG. After 18 h of induction in the dark the cells were harvested by centrifugation and the cell pellet was stored at -20°C until needed. The cell pellet containing WT or D76N mutant OaPAC was thawed and resuspended in resuspension buffer (50 mM NaH2PO4 pH 8.0, 300 mM NaCl, 2 mg/ml phenylmethylsulphonyl fluoride (PMSF), 1 mg/ml lysozyme, 0.5 mg/ml DNase, Pierce Protease inhibitor tablet (1 tablet/50 ml, Thermo Fisher Scientific)). The resuspended cells were disrupted and lysed by sonication at 4°C. The cell debris was removed by ultracentrifugation at 30,000 RPM for 80 min at 4°C. The supernatant was loaded onto a Ni-NTA column equilibrated with resuspension buffer. The column was washed with 60 mL of resuspension buffer containing 5 mM imidazole, and then the protein was eluted using resuspension buffer containing 500 mM imidazole. Buffer content of the eluate was immediately exchanged to 20 mM Tris, 150 mM NaCl pH 8.0, 20 mM MgCl2 using an Econo-Pac 10 G desalting column.

The protein was further purified with Superdex 200 column chromatography. Protein purity and yield were determined using SDS-PAGE and UV-Vis spectroscopy.

*Picosecond time-resolved fluorescence measurements*

Time-resolved fluorescence experiments in the ps time range were performed using a spectrally resolved Kerr-Gate femtosecond fluorometer. The setup employs a Kerr shutter and allows measuring fluorescence spectra with a temporal resolution down to ~100 fs and up to the nanoseconds timescale. The setup was described elsewhere(47). Briefly, the excitation pulse centered at 390 nm is obtained by frequency-doubling, using a BBO crystal, part of the 780 nm pulse operating at 1 kHz. The remaining 780 nm beam is led through a motorized delay-line and focused into the Kerr medium where it spatially overlapped the fluorescence from the sample. The Kerr medium used was $CS_2$ (response function width ~1.2 ps). The sample was flowed through the 1mm pathlength optical cell using a peristaltic pump. Transient fluorescence spectra were measured with time delays up to 1500 ps for all samples. Global analysis of the time and spectrally resolved data sets in terms of a linear combination of a discrete number of components, each with a distinct exponential rate constant and a decay-associated spectrum(51), was performed using Glotaran(52).

*Ultrafast Transient Absorption measurements*

Transient visible spectra were recorded with 100 fs temporal resolution by a transient absorption (TA) spectrometer applying ~800 μJ laser pulses centered at 800 nm at a repetition rate of 1 kHz. Ultrashort 100 fs pulses were obtained from a Spitfire Ace (Ti:sapphire) regenerative amplifier seeded by a femtosecond Mai Tai mode-locked (Ti:sapphire) laser oscillator and pumped by an Empower 45 multi-kilohertz, intracavity-doubled, green (Nd:YLF) pump laser. The output of the amplifier was split in the ratio 1:9 to build the so-called pump-probe arrangement. The higher energy pulses served to produce, in a BBO crystal, the SHG (second harmonic generation) 400nm pump pulses from the 800nm output of the regenerative amplifier and were attenuated to ~200-400nJ/pulse before reaching to the sample. The probe arm was provided by the lesser energy laser pulses via white continuum generation (WCG) in a rastered $CaF_2$ crystal. The pump and probe pulses were spatially overlapped in the sample and the polarization of the probe was again set to magic angle compared to excitation. To avoid

photodegradation, the cuvette was moved with the help of a homemade Lissajous scanner, simultaneously flowed by a peristaltic pump and kept at 12 °C temperature during the whole measurement. A Newport (IMS Series High-Performance Long Travel Linear Stages 600 PP) delay stage was placed in the beam path of the pump pulse to adjust the different pump-probe time delays. Exciting pulses were chopped by a Thorlabs MC2000 optical chopper (to half of the output repetition rate) to generate "pump ON" and "pump OFF" states of the sample. Absorption spectra were recorded by an Andor Newton CCD operating at -80 °C. Absorption data matrices were collected, and the absorption changes calculated, recorded and stored by the home written NI LabView (visual programming language) data acquisition and control software. The absorption changes were reported as pump on – pump off normalized difference spectra. The obtained data matrix was analysed by the Glotaran software assuming a sequential scheme with evolutionary associated spectra (EAS) assigned to the obtained time constants.

*cAMP yield measurement / Adenylate Cyclase Activity*

The ATP-cAMP conversion of WT and D67N mutant OaPAC was quantified using a pyrophosphate assay (EnzChek® Pyrophosphate Assay Kit). This assay is based on the PPi-dependent increase of the absorption of 2-amino-6-mercapto-7-methypurine, which was monitored as a function of time at 360 nm. The reaction rate was determined from the slope of a linear fit using an extinction coefficient of 11,000 $M^{-1}cm^{-1}$ at 360 nm. From the slope of the change of the absorbance the reaction rate (µM/s) of the purine base product (2-amino-6-mercapto-7-methypurine) was determined which is the same as the reaction rate of pyrophosphate derived from ATP.

To determine the Michaelis-Menten constant, the assay was performed on in the presence of 0-500 µM concentrations of ATP using the same condition of the continuous illumination. The initial reaction rate at each ATP concentration was extracted from the linear part of $OD_{360}$ vs. time plot. The resulting rate constants were plotted as a function of ATP concentration. Fitting a Michaelis-Menten saturation curve for the enzyme reaction, the maximum reaction rate ($V_{max}$), the concentration at the half of the maximum $K_M$ as well as the $k_{cat}$ – which is the number of ATP molecule each OaPAC converts to cAMP per unit time – were determined.

*Differential Scanning Calorimetry (DSC) measurements*

Differential scanning calorimetry (DSC) was performed to measure the thermal stability of the WT and D67N mutant OaPAC using a SETARAM Micro DSC-III calorimeter. The measurements were carried out in the range of 20 – 100 °C with a heating rate of 0.3 $K \cdot min^{-1}$. The sample (WT and D67N) and the reference (buffer) were balanced with a precision of ± 0.05 mg in order to avoid corrections for the heat capacity of the vessels. A second thermal scan of the denatured sample was measured for baseline correction. The melting temperature ($T_m$) of the thermal unfolding curves were analyzed by the OriginLab Origin®2021 software.

*Fluorescence anisotropy-based nucleotide-binding assays*

Fluorescence anisotropy-based nucleotide-binding assays were performed at room temperature using 2 µM 2'-(or-3')-O-(N-Methylanthraniloyl) Adenosine 5'-Triphosphate, Trisodium Salt (MANT ATP). This is a hydrolyzable fluorescently labelled ATP, on excitation at 350nm, emits at ~450nm. Steady-state fluorescence anisotropy measurements were performed with a Fluorolog Jobin Yvon Horiba spectrofluorometer in L-format configuration equipped with a polarization accessory. The measurements were performed at an excitation wavelength of λexc=350nm with a vertical polarization filter and by measuring the emission at 450nm (average of 30 measurements on the same sample) with the polarization filter both parallel and perpendicular with respect to the excitation light polarization. Fluorescence anisotropies were calculated from the fluorescence intensities detected according to the equation (1)

$$\boldsymbol{r} = \frac{\boldsymbol{I_{perp/perp} - G(\lambda) I_{perp/par}}}{\boldsymbol{I_{perp/perp} + 2G(\lambda) I_{perp/par}}} \qquad (1)$$

where r is the fluorescence anisotropy, $I_{perp/perp}$ is the fluorescence emission intensity detected with vertical polarization, $I_{perp/par}$ is the fluorescence emission intensity detected with vertical polarization on the excitation and horizontal polarization on the emission, and G(λ) is the correction factor experimentally determined measuring the ratio $I_{perp}/I_{par}$ with a horizontally polarized excitation. Data processing was done using Origin 2020 software (OriginLab) and $K_D$ values were determined by fitting to a quadratic binding equation

$$\frac{r - r_A}{r_{AT} - r_A} = \frac{A_0 + T_0 + K_D - \sqrt{(A_0 + T_0 + K_D)^2 - 4 \cdot A_0 \cdot T_0}}{2} \qquad (2)$$

where $A_o$ and $T_o$ are the total MANT-ATP/cAMP and OaPAC concentrations respectively, $r_A$ is the steady-state anisotropy of MANT-ATP/cAMP, $r_{AT}$ is the steady-state anisotropy of MANT-ATP/cAMP at a saturating amount of OaPAC and $K_D$ is the dissociation equilibrium constant of the MANT-ATP/cAMP-OaPAC complex.

**Data availability statement**

Data are available in the Supporting information. All remaining data are contained in the article.

**Acknowledgements**

J.T.C. was supported by the National Institutes of Health IMSD-MERGE (T32GM135746) and NY-CAPs IRACDA (K12-GM102778) Programs at Stony Brook University. B.Z. was supported by a PhD scholarship from the Chinese scholarship Council. A.L. acknowledges funding from the Hungarian National Research and Innovation Office (K-137557) and was supported by PTE ÁOK-KA-2021. This study was supported by the National Science Foundation (NSF) (MCB-1817837 to PJT) and the EPSRC (EP/N033647/1 to S.R.M.).

## References


1. Ohki, M., Sugiyama, K., Kawai, F., Matsunaga, S., Iseki, M., andPark, S. (2016) Structural basis for photoactivation of a light-regulated adenylate cyclase from the photosynthetic cyanobacterium Oscillatoria acuminata Acta Crystallographica a-Foundation and Advances **72**, S251-S251 10.1107/S2053273316096194
2. Anderson, S., Dragnea, V., Masuda, S., Ybe, J., Moffat, K., andBauer, C. (2005) Structure of a novel photoreceptor, the BLUF domain of AppA from Rhodobacter sphaeroides Biochemistry **44**, 7998-8005 10.1021/bi0502691
3. Masuda, S., Hasegawa, K., Ishii, A., andOno, T. A. (2004) Light-induced structural changes in a putative blue-light receptor with a novel FAD binding fold sensor of blue-light using FAD (BLUF); Slr1694 of synechocystis sp. PCC6803 Biochemistry **43**, 5304-5313 10.1021/bi049836v
4. Bonetti, C., Mathes, T., van Stokkum, I., van Grondelle, R., Groot, M., Hegemann, P. *et al.* (2007) The light activation mechanism of a novel blue-light photoreceptor Biophysical Journal 337A-337A
5. Bonetti, C., Stierl, M., Mathes, T., van Stokkum, I., Mullen, K., Cohen-Stuart, T. *et al.* (2009) The Role of Key Amino Acids in the Photoactivation Pathway of the Synechocystis Slr1694 BLUF Domain Biochemistry **48**, 11458-11469 10.1021/bi901196x
6. Gauden, M., Yeremenko, S., Laan, W., van Stokkum, I., Ihalainen, J., van Grondelle, R. *et al.* (2005) Photocycle of the flavin-binding photoreceptor AppA, a bacterial transcriptional antirepressor of photosynthesis genes Biochemistry **44**, 3653-3662 10.1021/bi047359a
7. Mathes, T., van Stokkum, I., Bonetti, C., Hegemann, P., andKennis, J. (2011) The Hydrogen-Bond Switch Reaction of the Blrb Bluf Domain of Rhodobacter sphaeroides Journal of Physical Chemistry B **115**, 7963-7971 10.1021/jp201296m
8. Lukacs, A., Tonge, P. J., andMeech, S. R. (2022) Photophysics of the Blue Light Using Flavin Domain Acc Chem Res **55**, 402-414 10.1021/acs.accounts.1c00659
9. Zhong, D., andZewail, A. H. (2001) Femtosecond dynamics of flavoproteins: charge separation and recombination in riboflavine (vitamin B2)-binding protein and in glucose oxidase enzyme Proc Natl Acad Sci U S A **98**, 11867-11872 10.1073/pnas.211440398
10. Nag, L., Lukacs, A., andVos, M. H. (2019) Short-Lived Radical Intermediates in the Photochemistry of Glucose Oxidase Chemphyschem **20**, 1793-1798 10.1002/cphc.201900329
11. Mataga, N., Chosrowjan, H., Shibata, Y., Tanaka, F., Nishina, Y., andShiga, K. (2000) Dynamics and mechanisms of ultrafast fluorescence quenching reactions of flavin chromophores in protein nanospace Journal of Physical Chemistry B **104**, 10667-10677 10.1021/jp002145y
12. Müller, P., Bouly, J. P., Hitomi, K., Balland, V., Getzoff, E. D., Ritz, T. *et al.* (2014) ATP binding turns plant cryptochrome into an efficient natural photoswitch Sci Rep **4**, 5175 10.1038/srep05175
13. Müller, P., andBouly, J. P. (2015) Searching for the mechanism of signalling by plant photoreceptor cryptochrome FEBS Lett **589**, 189-192 10.1016/j.febslet.2014.12.008
14. Müller, P., Brettel, K., Grama, L., Nyitrai, M., andLukacs, A. (2016) Photochemistry of Wild-Type and N378D Mutant E. coli DNA Photolyase with Oxidized FAD Cofactor Studied by Transient Absorption Spectroscopy Chemphyschem **17**, 1329-1340 10.1002/cphc.201501077
15. Kottke, T., Hense, A., Herman, E., andOldemeyer, S. (2015) Proton Transfer to Flavin Stabilizes the Signaling State of the Blue Light Receptor Plant Cryptochrome Faseb Journal **29**,
16. Langenbacher, T., Immeln, D., Dick, B., andKottke, T. (2009) Microsecond Light-induced Proton Transfer to Flavin in the Blue Light Sensor Plant Cryptochrome Journal of the American Chemical Society **131**, 14274-14280 10.1021/ja901628y
17. Lukacs, A., Brust, R., Haigney, A., Laptenok, S. P., Addison, K., Gil, A. *et al.* (2014) BLUF domain function does not require a metastable radical intermediate state J Am Chem Soc **136**, 4605-4615 10.1021/ja4121082
18. Brust, R., Haigney, A., Lukacs, A., Gil, A., Hossain, S., Addison, K. *et al.* (2014) Ultrafast Structural Dynamics of BlsA, a Photoreceptor from the Pathogenic Bacterium J Phys Chem Lett **5**, 220-224 10.1021/jz4023738

19. Gil, A. A., Laptenok, S. P., Iuliano, J. N., Lukacs, A., Verma, A., Hall, C. R. *et al.* (2017) Photoactivation of the BLUF Protein PixD Probed by the Site-Specific Incorporation of Fluorotyrosine Residues J Am Chem Soc **139**, 14638-14648 10.1021/jacs.7b07849
20. Fujisawa, T., Takeuchi, S., Masuda, S., andTahara, T. (2014) Signaling-State Formation Mechanism of a BLUF Protein PapB from the Purple Bacterium Rhodopseudomonas palustris Studied by Femtosecond Time-Resolved Absorption Spectroscopy J Phys Chem B **118**, 14761-14773 10.1021/jp5076252
21. Stelling, A. L., Ronayne, K. L., Nappa, J., Tonge, P. J., andMeech, S. R. (2007) Ultrafast Structural Dynamics in BLUF Domains: Transient Infrared Spectroscopy of AppA and Its Mutants JACS **129**, 15556-15564 10.1021/ja074074n
22. Lukacs, A., Haigney, A., Brust, R., Zhao, R. K., Stelling, A. L., Clark, I. P. *et al.* (2011) Photoexcitation of the blue light using FAD photoreceptor AppA results in ultrafast changes to the protein matrix J Am Chem Soc **133**, 16893-16900 10.1021/ja2060098
23. Khrenova, M. G., Domratcheva, T., Schlichting, I., Grigorenko, B. L., andNemukhin, A. V. (2011) Computational characterization of reaction intermediates in the photocycle of the sensory domain of the AppA blue light photoreceptor Photochem Photobiol **87**, 564-573 10.1111/j.1751-1097.2010.00861.x
24. Khrenova, M. G., Nemukhin, A. V., andDomratcheva, T. (2013) Photoinduced electron transfer facilitates tautomerization of the conserved signaling glutamine side chain in BLUF protein light sensors J Phys Chem B **117**, 2369-2377 10.1021/jp312775x
25. Sadeghian, K., Bocola, M., andSchütz, M. (2008) A conclusive mechanism of the photoinduced reaction cascade in blue light using flavin photoreceptors J Am Chem Soc **130**, 12501-12513 10.1021/ja803726a
26. Udvarhelyi, A., andDomratcheva, T. (2011) Photoreaction in BLUF receptors: proton-coupled electron transfer in the flavin-Gln-Tyr system Photochem Photobiol **87**, 554-563 10.1111/j.1751-1097.2010.00884.x
27. Udvarhelyi, A., andDomratcheva, T. (2013) Glutamine rotamers in BLUF photoreceptors: a mechanistic reappraisal J Phys Chem B **117**, 2888-2897 10.1021/jp400437x
28. Hsiao, Y. W., Götze, J. P., andThiel, W. (2012) The central role of Gln63 for the hydrogen bonding network and UV-visible spectrum of the AppA BLUF domain J Phys Chem B **116**, 8064-8073 10.1021/jp3028758
29. Hontani, Y., Mehlhorn, J., Domratcheva, T., Beck, S., Kloz, M., Hegemann, P. *et al.* (2023) Spectroscopic and Computational Observation of Glutamine Tautomerization in the Blue Light Sensing Using Flavin Domain Photoreaction J Am Chem Soc **145**, 1040-1052 10.1021/jacs.2c10621
30. Domratcheva, T., Hartmann, E., Schlichting, I., andKottke, T. (2016) Evidence for Tautomerisation of Glutamine in BLUF Blue Light Receptors by Vibrational Spectroscopy and Computational Chemistry Sci Rep **6**, 22669 10.1038/srep22669
31. Goings, J., Li, P., Zhu, Q., andHammes-Schiffer, S. (2020) Formation of an unusual glutamine tautomer in a blue light using flavin photocycle characterizes the light-adapted state Proceedings of the National Academy of Sciences of the United States of America **117**, 26626-26632 10.1073/pnas.2016719117
32. Nagahama, T., Suzuki, T., Yoshikawa, S., andIseki, M. (2007) Functional transplant of photoactivated adenylyl cyclase into Aplysia mechanosensory neurons Neuroscience Research **58**, S241-S241 10.1016/j.neures.2007.06.593
33. Jansen, V., Alvarez, L., Balbach, M., Strunker, T., Hegemann, P., Kaupp, U. *et al.* (2015) Controlling fertilization and cAMP signaling in sperm by optogenetics Elife **4**, 10.7554/eLife.05161
34. Lindner, R., Hartmann, E., Tarnawski, M., Winkler, A., Frey, D., Reinstein, J. *et al.* (2017) Photoactivation Mechanism of a Bacterial Light-Regulated Adenylyl Cyclase Journal of Molecular Biology **429**, 1336-1351 10.1016/j.jmb.2017.03.020
35. Collado, J., Iuliano, J., Pirisi, K., Jewlikar, S., Adamczyk, K., Greetham, G. *et al.* (2022) Unraveling the Photoactivation Mechanism of a Light-Activated Adenylyl Cyclase Using Ultrafast Spectroscopy Coupled with Unnatural Amino Acid Mutagenesis Acs Chemical Biology **17**, 2643-2654 10.1021/acschembio.2c00575
36. Lakowicz, J. R. (2006) *Principles of fluorescence spectroscopy*, Springer,
37. Bonetti, C., Mathes, T., van Stokkum, I. H., Mullen, K. M., Groot, M. L., van Grondelle, R. *et al.* (2008) Hydrogen bond switching among flavin and amino acid side chains in the BLUF photoreceptor observed by ultrafast infrared spectroscopy Biophys J **95**, 4790-4802 10.1529/biophysj.108.139246
38. Goings, J., andHammes-Schiffer, S. (2019) Early Photocycle of Slr1694 Blue-Light Using Flavin Photoreceptor Unraveled through Adiabatic Excited-State Quantum Mechanical/Molecular Mechanical Dynamics Journal of the American Chemical Society **141**, 20470-20479 10.1021/jacs.9b11196

39. Lukacs, A., Eker, A., Byrdin, M., Villette, S., Pan, J., Brettel, K. *et al.* (2006) Role of the middle residue in the triple tryptophan electron transfer chain of DNA photolyase: Ultrafast spectroscopy of a Trp -> Phe mutant Journal of Physical Chemistry B **110**, 15654-15658 10.1021/jp063686b
40. Lukacs, A., Eker, A. P., Byrdin, M., Brettel, K., andVos, M. H. (2008) Electron hopping through the 15 A triple tryptophan molecular wire in DNA photolyase occurs within 30 ps J Am Chem Soc **130**, 14394-14395 10.1021/ja805261m
41. Zhuang, B., Liebl, U., andVos, M. H. (2022) Flavoprotein Photochemistry: Fundamental Processes and Photocatalytic Perspectives J Phys Chem B **126**, 3199-3207 10.1021/acs.jpcb.2c00969
42. Zhuang, B., Vos, M. H., andAleksandrov, A. (2022) Photochemical and Molecular Dynamics Studies of Halide Binding in Flavoenzyme Glucose Oxidase Chembiochem **23**, e202200227 10.1002/cbic.202200227
43. Zhuang, B., Ramodiharilafy, R., Liebl, U., Aleksandrov, A., andVos, M. H. (2022) Ultrafast photooxidation of protein-bound anionic flavin radicals Proc Natl Acad Sci U S A **119**, 10.1073/pnas.2118924119
44. Kao, Y., Saxena, C., He, T., Guo, L., Wang, L., Sancar, A. *et al.* (2008) Ultrafast dynamics of flavins in five redox states Journal of the American Chemical Society **130**, 13132-13139 10.1021/ja8045469
45. Brazard, J., Usman, A., Lacombat, F., Ley, C., Martin, M. M., Plaza, P. *et al.* (2010) Spectro-temporal characterization of the photoactivation mechanism of two new oxidized cryptochrome/photolyase photoreceptors J Am Chem Soc **132**, 4935-4945 10.1021/ja1002372
46. Nag, L., Sournia, P., Myllykallio, H., Liebl, U., andVos, M. (2017) Identification of the TyrOH(center dot+) Radical Cation in the Flavoenzyme TrmFO (vol 139, pg 11500, 2017) Journal of the American Chemical Society **139**, 15554-15554 10.1021/jacs.7b10508
47. Laptenok, S. P., Nuernberger, P., Lukacs, A., andVos, M. H. (2014) Subpicosecond Kerr-gate spectrofluorometry Methods Mol Biol **1076**, 321-336 10.1007/978-1-62703-649-8_13
48. Karadi, K., Kapetanaki, S. M., Raics, K., Pecsi, I., Kapronczai, R., Fekete, Z. *et al.* (2020) Functional dynamics of a single tryptophan residue in a BLUF protein revealed by fluorescence spectroscopy Sci Rep **10**, 2061 10.1038/s41598-020-59073-5
49. Zhou, Z., Chen, Z., Kang, X. W., Zhou, Y., Wang, B., Tang, S. *et al.* (2022) The nature of proton-coupled electron transfer in a blue light using flavin domain Proc Natl Acad Sci U S A **119**, e2203996119 10.1073/pnas.2203996119
50. Gil, A., Haigney, A., Laptenok, S. P., Brust, R., Lukacs, A., Iuliano, J. *et al.* (2016) Mechanism of the AppABLUF Photocycle Probed by Site-Specific Incorporation of Fluorotyrosine Residues: Effect of the Y21 pKa on the Forward and Reverse Ground-State Reactions J Am Chem Soc **138**, 926-935 10.1021/jacs.5b11115
51. van Stokkum, I. H., Larsen, D. S., andvan Grondelle, R. (2004) Global and target analysis of time-resolved spectra Biochim Biophys Acta **1657**, 82-104 10.1016/j.bbabio.2004.04.011
52. Snellenburg, J., Laptenok, S., Seger, R., Mullen, K., andvan Stokkum, I. (2012) Glotaran: A Java-Based Graphical User Interface for the R Package TIMP Journal of Statistical Software **49**, 1-22 10.18637/jss.v049.i03

## Figure legends

**Figure 1.**

Environment of FAD in OaPAC including the Y6, D67, Q48 and W90 amino acids, involved in the photophysics of OaPAC (PDB: 4yus). Y6 is the primary electron donor, but W90 can donate an electron as well. Q48 is crucial in the propagation of the signal from the BLUF domain towards the AC domain. D67 is in hydrogen bonding distance to R79 (~3 Å) residue and to the ribityl chain (~3.2 Å) of flavin. D67 is a hydrogen bond acceptor and mutating D67 to N, a neutral amino acid, modulates the electrostatic potential of flavin by altering the hydrogen boding network.

**Figure 2.**

A) Transient absorption measurements on the D67N mutant at indicated time delays B) EAS spectra obtained after global analysis. The time constants show that the excited state of FAD, formed right after excitation, decays in 5 ps to the next state which shows the presence of the neutral flavin radical. The final state is dominated by the signalling state and exist longer then the window of the measurement C) Individual kinetics of the WT and D67N OaPAC measured at 505 nm. Applying a monoexponential fit the time constants for the WT and D67N were 90 ± 30 ps and 64 ± 8 ps respectively

**Figure 3.**

A) EAS spectra obtained by global analysis of the transient fluorescence data of WT. The result of the global fit shows a heterogenous decay of the flavin. B) EAS spectra obtained by global analysis of the transient fluorescence data of the D67N mutant. C) Individual kinetics of the fluorescence decay observed at 513 nm. Using a monoexponential fit we obtained a fluorescence lifetime of 40 ± 2 ps for WT and 25 ± 2 ps for D67N.

**Figure 4.**

A) The kinetics of ATP conversion in the dark- and light-adapted state of WT and D67N OaPAC. In the dark, the ATP conversion rate is slightly higher in the D67N mutant (green) than in WT (orange). In the light-adapted state at 0.5 mM ATP the speed of the conversion was higher in the case of the mutant (blue) than in WT (red). B) Michelis-Menten plot of

the enzymatic activity of WT (red) and D67N (blue) under irradiation, $v_{max}$ is increased in the D67N mutant.

**Figure 5.**

A) Absorption spectra of WT and D67N OaPAC in dark and light state. The absorption spectra of WT and the mutant are very similar in the dark adapted state: the peak of the $S_0$-$S_1$ transition is the same for both proteins with a maximum at 442 nm; a 4 nm blue shift of the $S_0$-$S_2$ transition is observed for the mutant (376 nm for the WT and 372 nm for the mutant). In light adapted state the $S_0$-$S_1$ peak shifts to 452 nm in WT and to 456 nm in the mutant. The $S_0$-$S_2$ peak shifts from 376 nm to 379 nm in the WT, and from 372 nm to 376 nm in the mutant. B) Recovery kinetics of WT (red) and D67N (blue) OaPAC, measured at 490 nm The time constant of dark state recovery is 3.6 s for WT and 15.3 s for D67N

**Figure 6.**

Thermal unfolding of wild type (WT) and mutant (D67N) OaPAC measured by DSC. The DSC curve of the WT shows a steep endothermic unfolding with a melting temperature of 6 $^{o}$C higher than of the mutant. This points to a more stable or packed structure of the WT protein as denaturing starts at lower temperature in the case of the mutant.

**Figure 7.**

Fluorescence anisotropy measurement of MANT-ATP nucleotide in WT and D67N OaPAC as a function of protein concentration at fixed (1 μM) MANT-ATP concentration. As the concentration of protein is increasing the population of bound nucleotide is also increase resulting in higher fluorescence anisotropy. The obtained binding affinity from the fit was 2.2 ± 0.4 μM in WT and 7.7 ± 1.6 μM in D67N.

**Table 1**.

Kinetic parameters for wild-type OaPAC and D67N mutant.

Figure 1

Click here to access/download;Main Figure (High Resolution);Fig 1_modified.tif

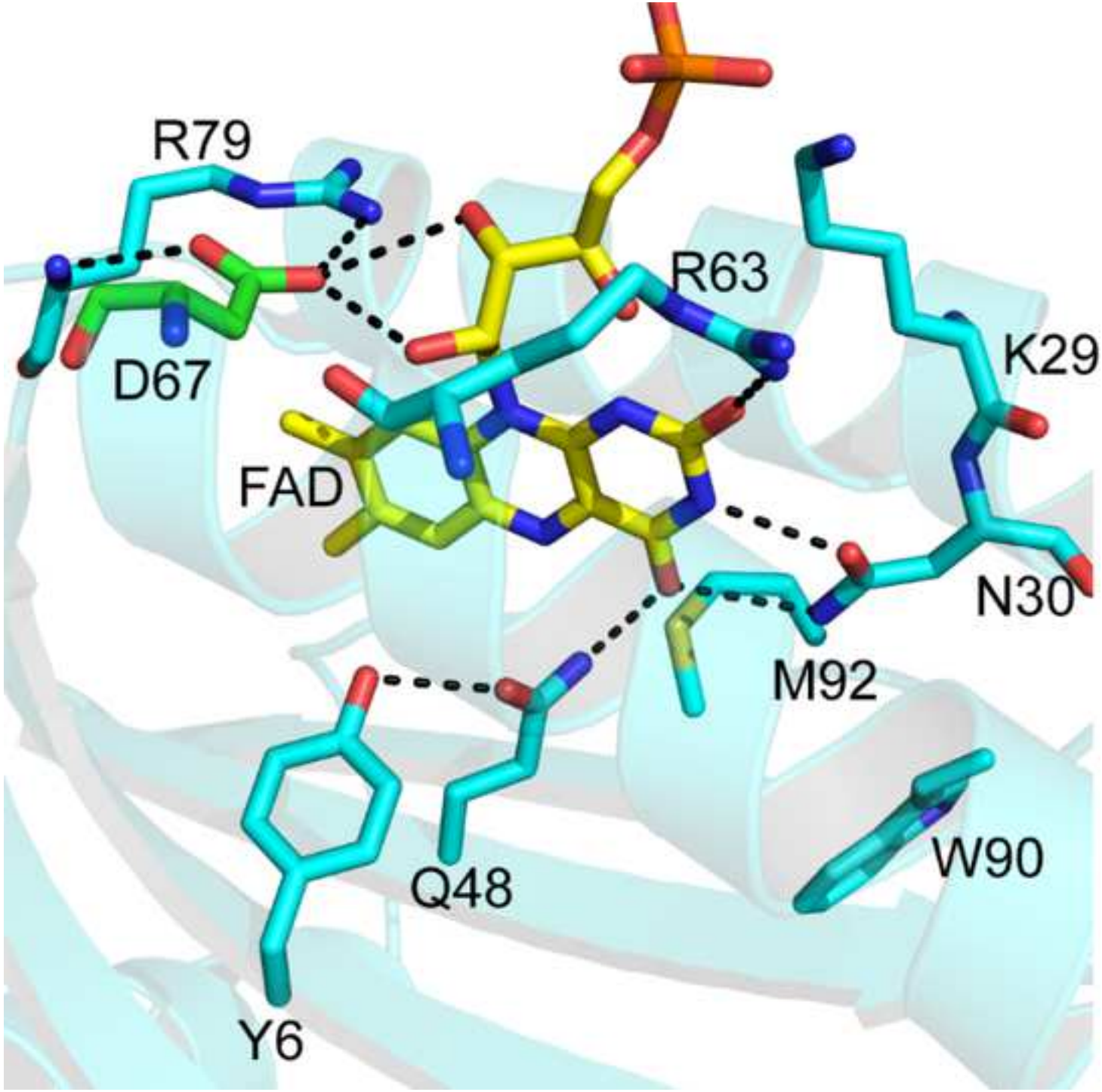

Figure 2

Click here to access/download;Main Figure (High Resolution);Figure 2. ABC.tif

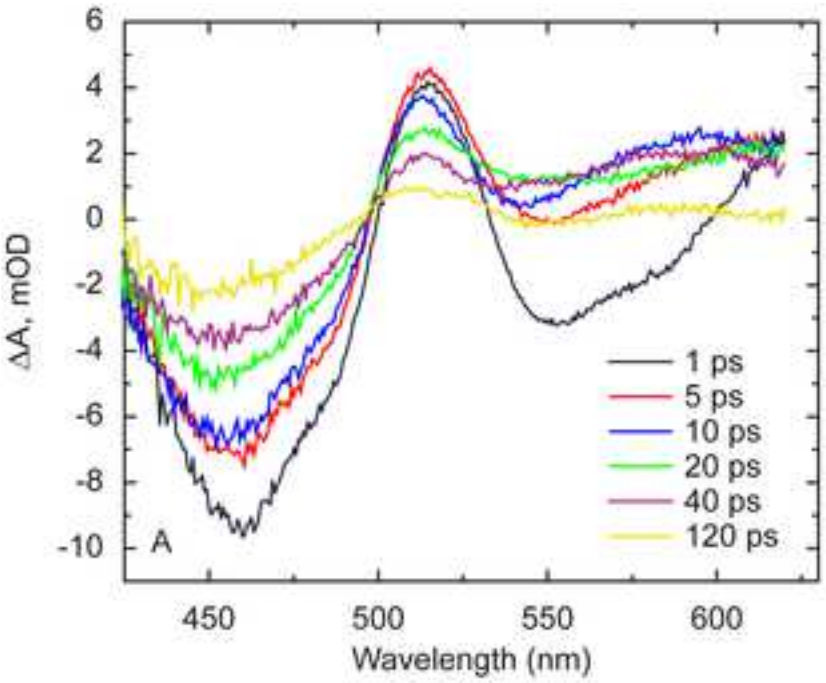


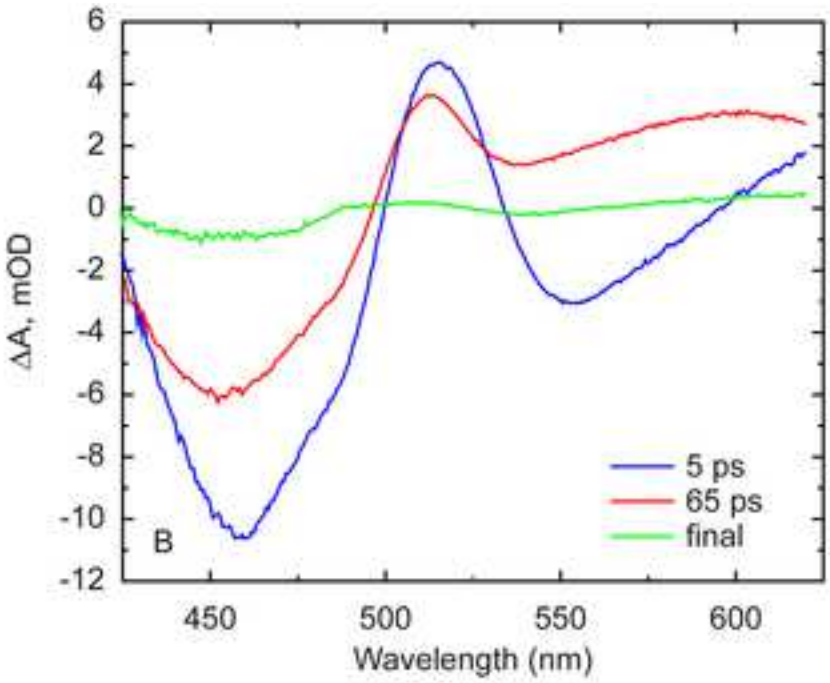


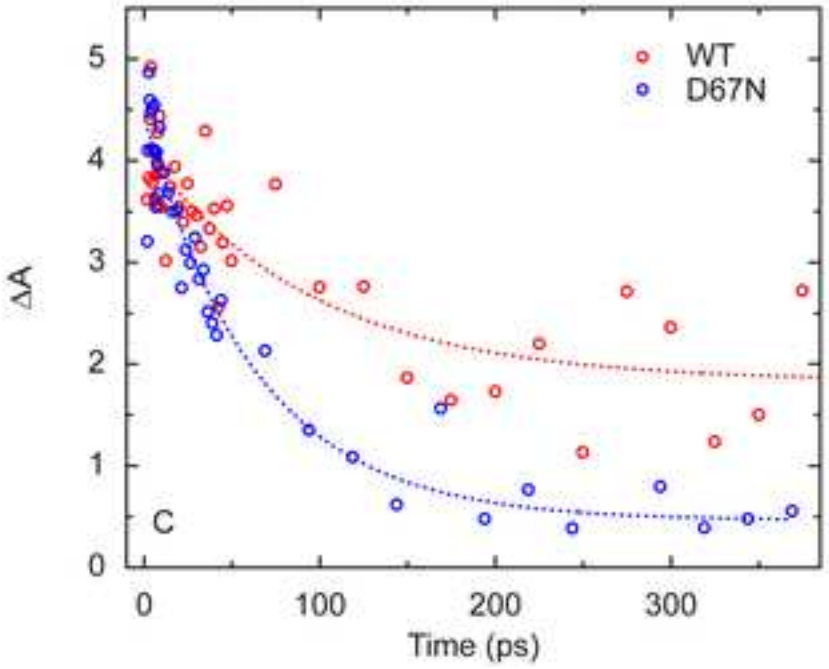

Figure 3

Click here to access/download;Main Figure (High Resolution);Figure 3. ABC new.tif

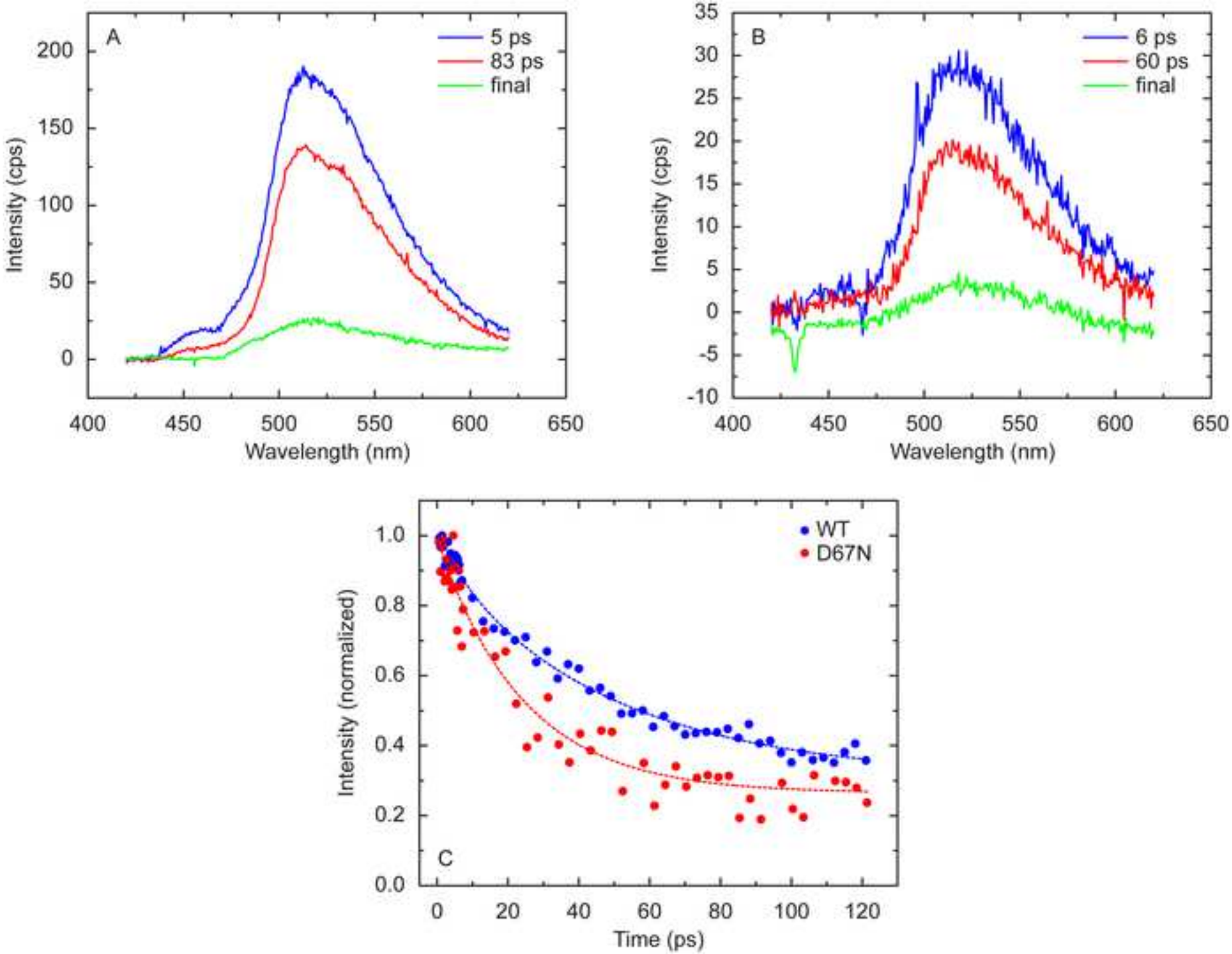

Figure 4

Click here to access/download;Main Figure (High Resolution);Figure 4AB.tif

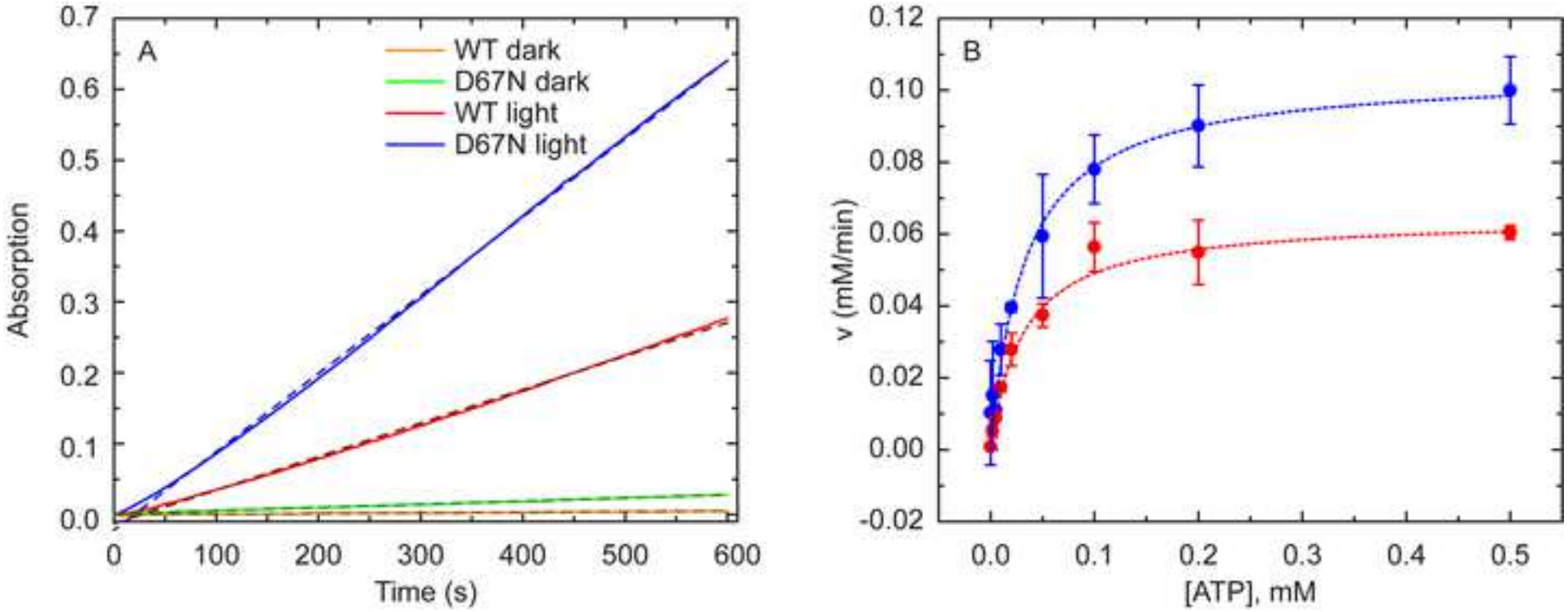

Figure 5

Click here to access/download;Main Figure (High Resolution);Figure 5AB.tif

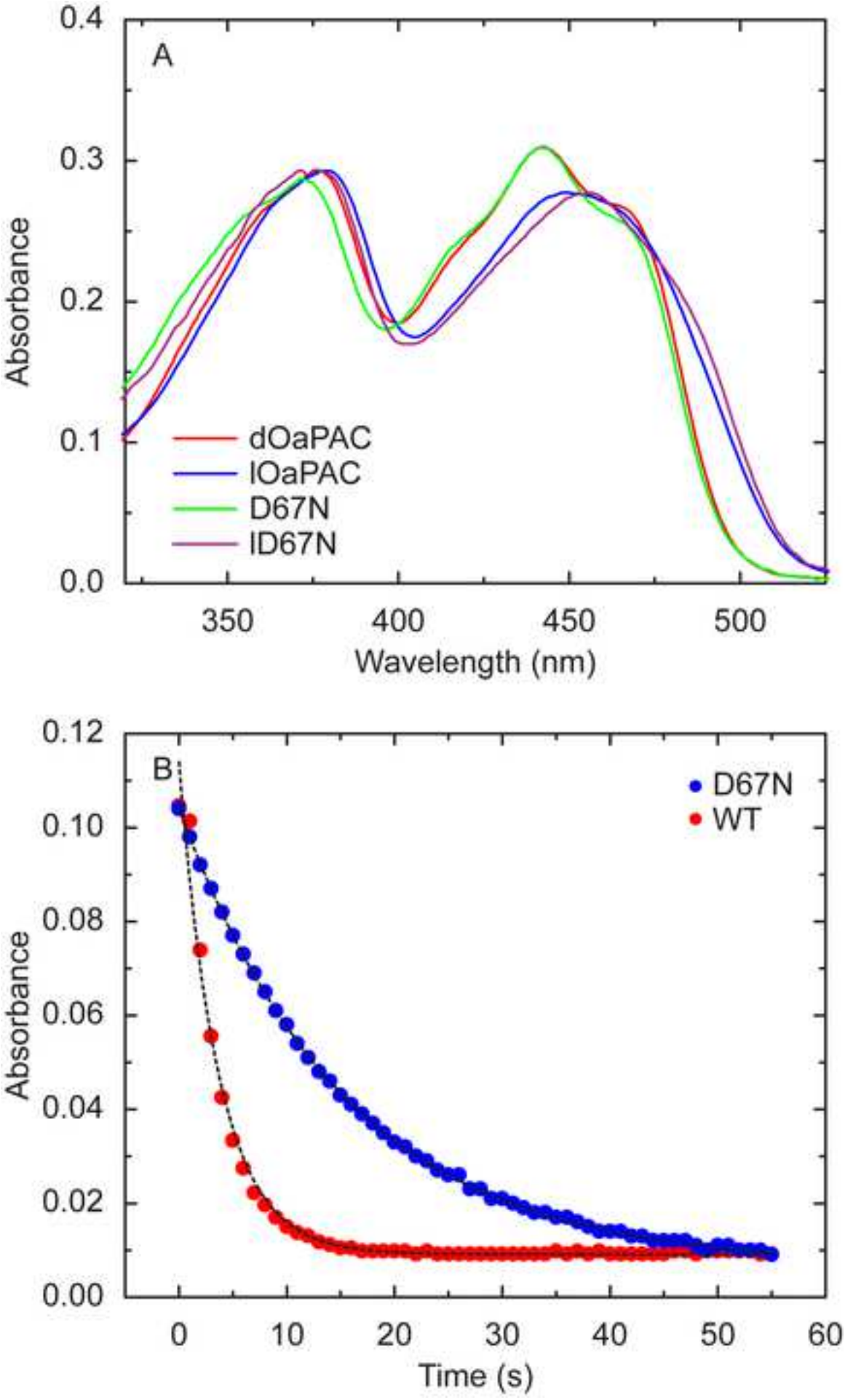

Figure 6

Click here to access/download;Main Figure (High Resolution);Figure 6.tif

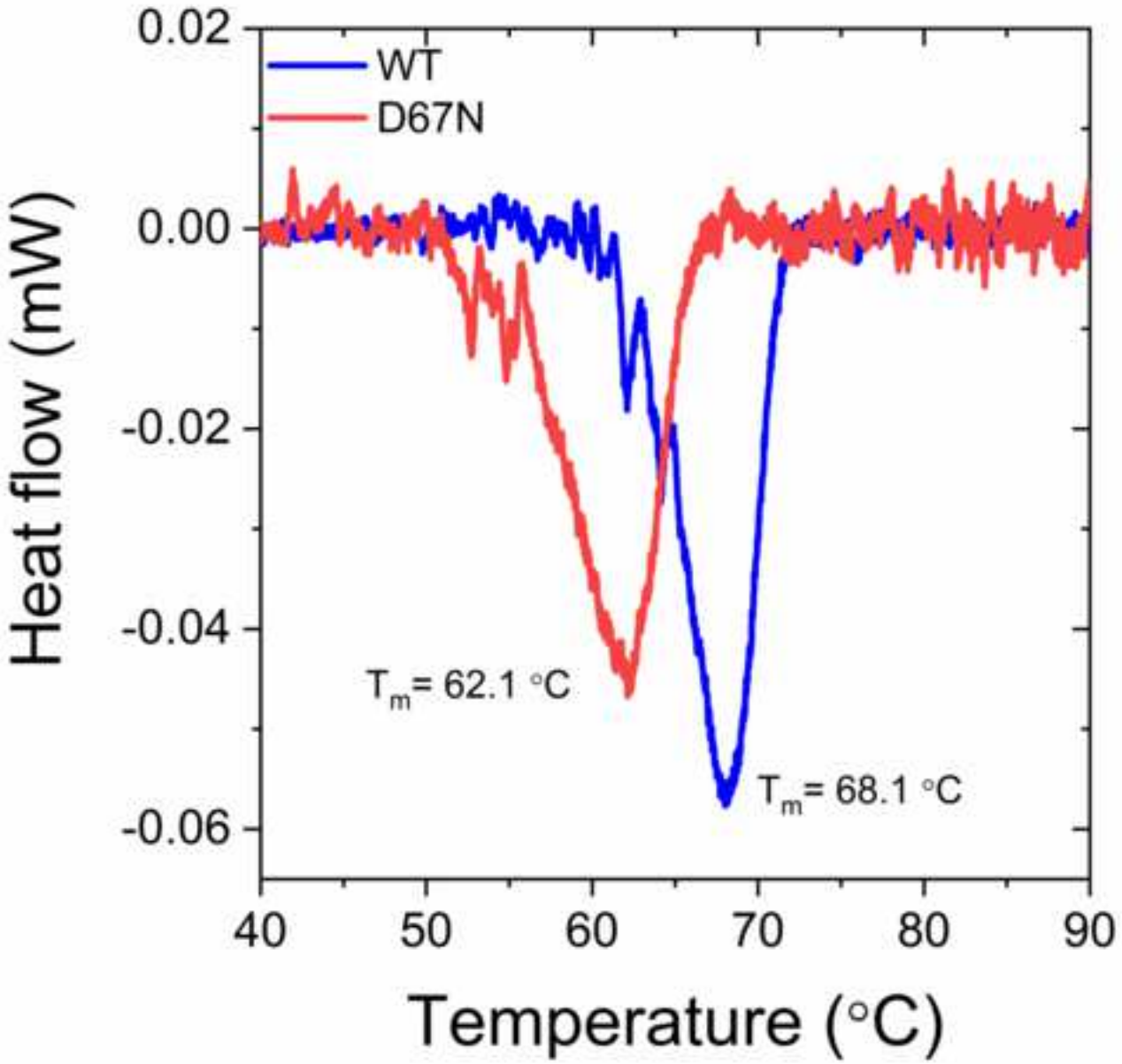

Click here to access/download;Main Figure (High Resolution);Fig7 modified.tif

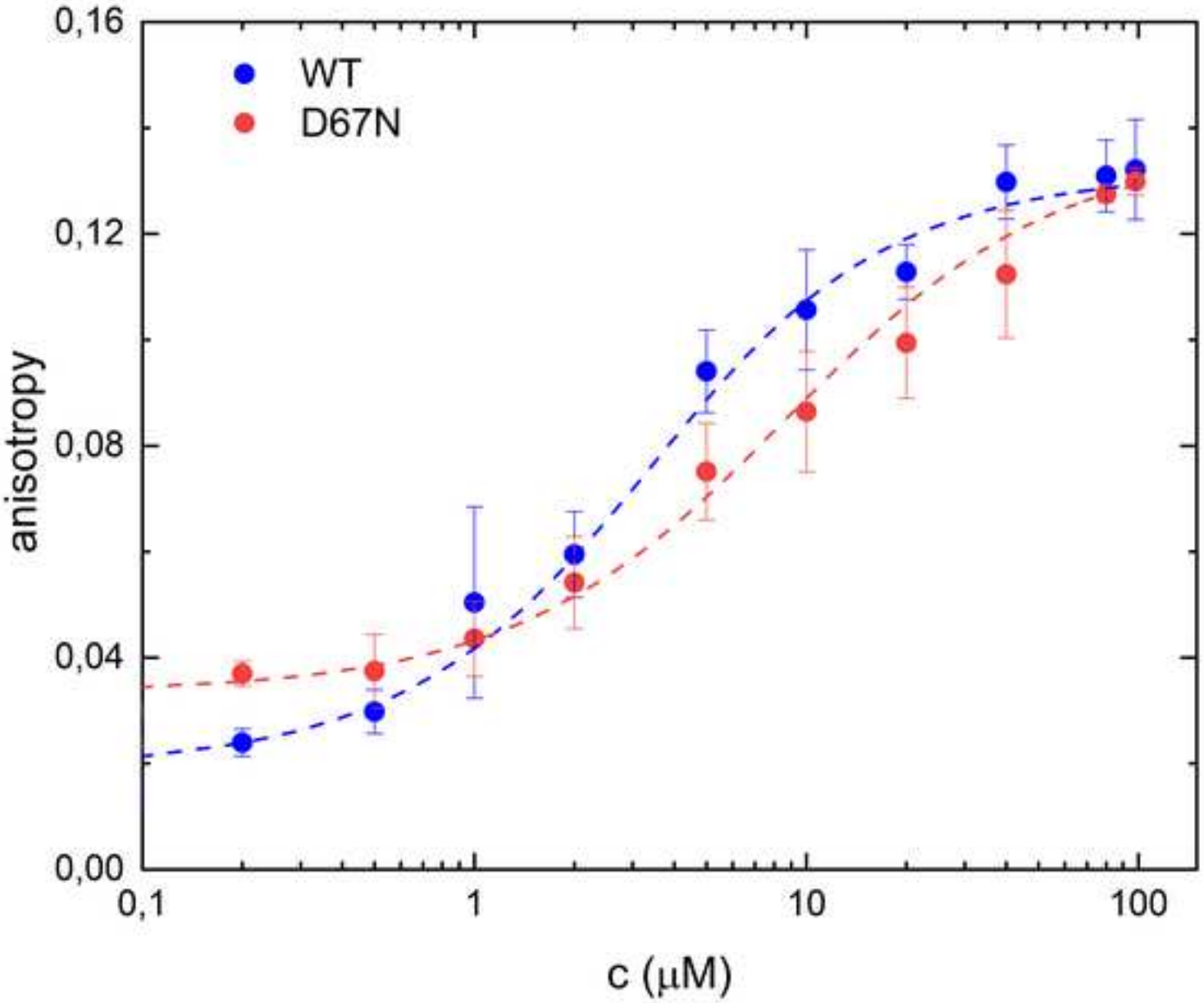

Table 1

| Parameters | WT OaPAC | D67N mutant |
|---|---|---|
| $v_{max}$ | 0.064 ± 0.007 mM/min | 0.100±0.002 mM /min |
| $k_{cat}$ | 32.2 1/min | 50.05 1/min |
| $K_M$ | 0.031 ± 0.001 mM | 0.041 ± 0.005 mM |
| Dark state recovery | 3.6 s | 15.3 s |
| Excited state relaxation | 90 ± 30 ps | 64 ± 8 ps |
| Fluorescence lifetime | 40 ± 2 ps | 25 ± 2 ps |
| $T_m$ | 68.1 ºC | 62.1 ºC |
| ΔH | 0.078 J/g | 0.069 J/g |
| Kd | 2.2 ± 0.4 mM | 7.7 ± 1.6 mM |

Credit author statement

**Katalin Raics**: Investigation, Data analysis **Katalin Pirisi**: Investigation **Yin Li**: Investigation **Bo Zhuang**: Investigation, Data Analysis **Zsuzsanna Fekete**: Investigation, Methodology **Nikolett Kis-Bicskei:** Investigation, Methodology, **Ildiko Pecsi**: Investigation, Methodology **Kinga Pozsonyi Ujfalusi**: Investigation, **Elek Telek:** Investigation **Jinnette Tolentino Collado:** Investigation, Visualization **Peter J. Tonge**: Conceptualization, Writing **Stephen R. Meech**: Conceptualization, Writing, **Marten H. Vos** : Investigation, Writing **Emoke Bodis**: Investigation, Data analysis **Andras Lukacs:** Conceptualization, Investigation, Writing

## 1. Spectral modelling of the transient absorption spectra

In order to find the presence of the different radical species we used reference spectra of each plausible radical. The flavin radical spectra were taken from measurements performed on mosquito AgCRY1 (*Anopheles gambiae*). (1, 2) Fig. S1 also contains the spectra of tryptophan radicals determined by pulsed radiolysis experiments.(3) The EAS2 (65 ps) spectra could be fit with a combination of spectra of the flavin excited state and the neutral radical state.

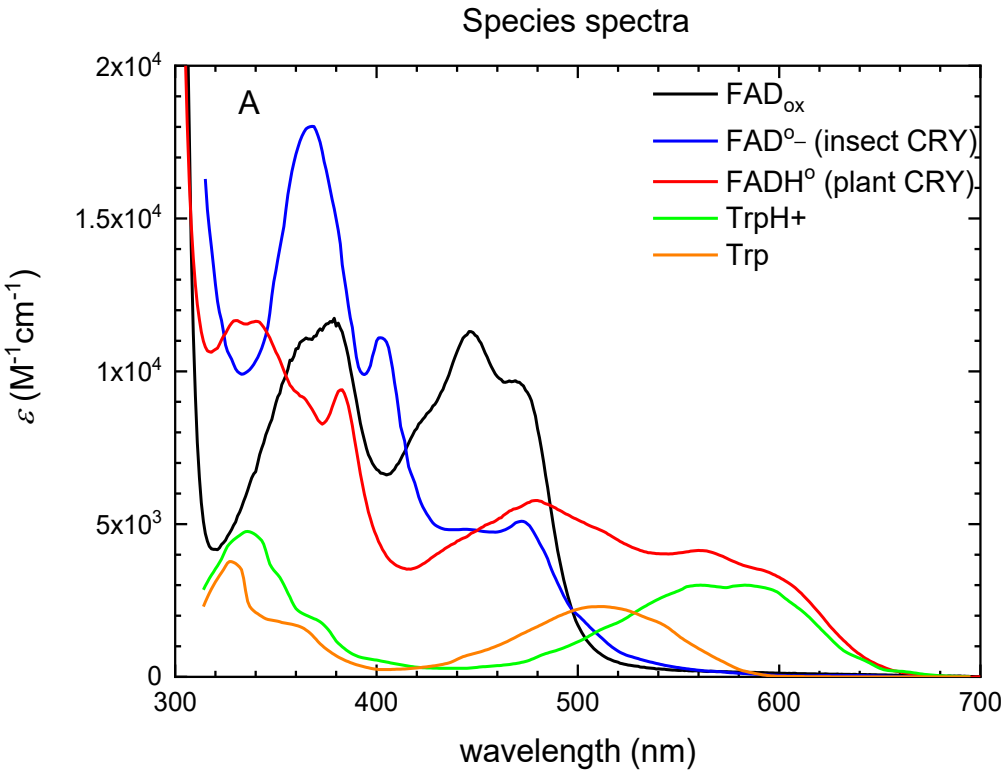

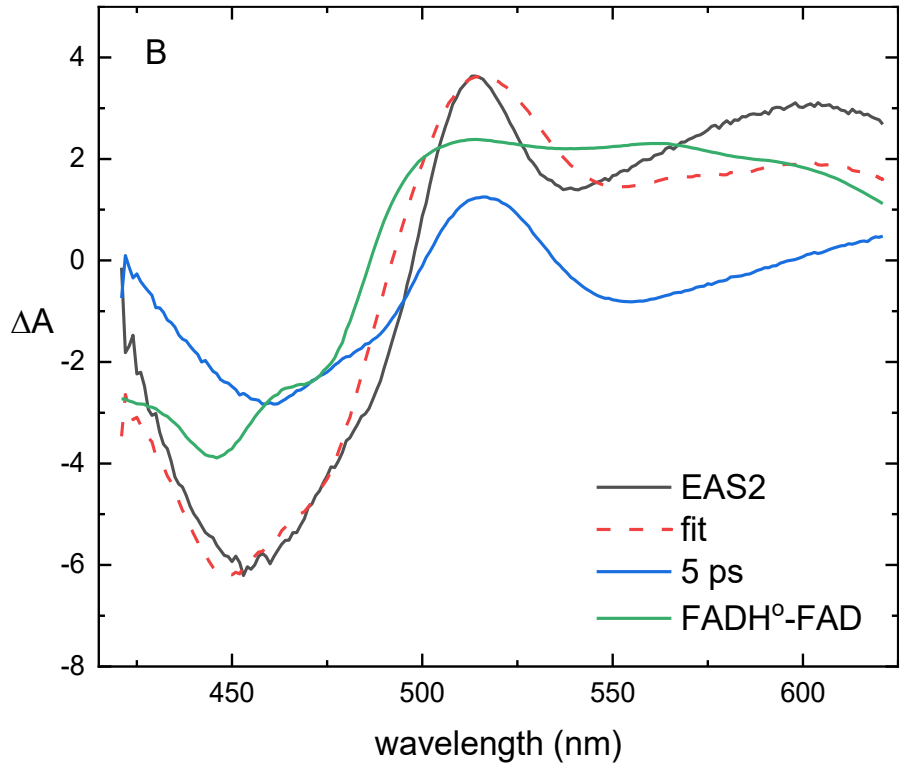


**Figure S1**. Spectral fitting of **A)** Spectra of the oxidized FAD and the radical FAD species as well as the spectra of the tryptophan radicals. As TyrH and Tyr° do not absorb at >420 nm, their contributions were not taken into account. **B)** 65 ps component for D67N-OaPAC was fitted as a linear combination of (FADH°–FAD) and (FAD*-$FAD_{ox}$) spectra, as from the fluorescence measurements can be seen that the excited state is present at the longer time constant as well. The FADH° and $FAD_{ox}$ spectra from fig S1A were used to construct the (FADH°–FAD) spectrum and the 5-ps EAS was used as (FAD*-$FAD_{ox}$) spectrum.

## 2. PixD WT and D69N fluorescence data

To check the effect of the mutation proposed by Goings et al.(4) in PixD we made the mutant and performed transient fluorescent measurement on WT as well as on the D69N mutant. The fluorescence decay of WT PixD was heterogeneous, similar to WT OaPAC with longer time constants. The time constants of the D69N mutant were very close to the observed in OaPAC D67N mutant. Observing the fluorescence decay of WT and D69N at 520 nm, one can see only a slightly faster initial decay of the fluorescence emission in the mutant.

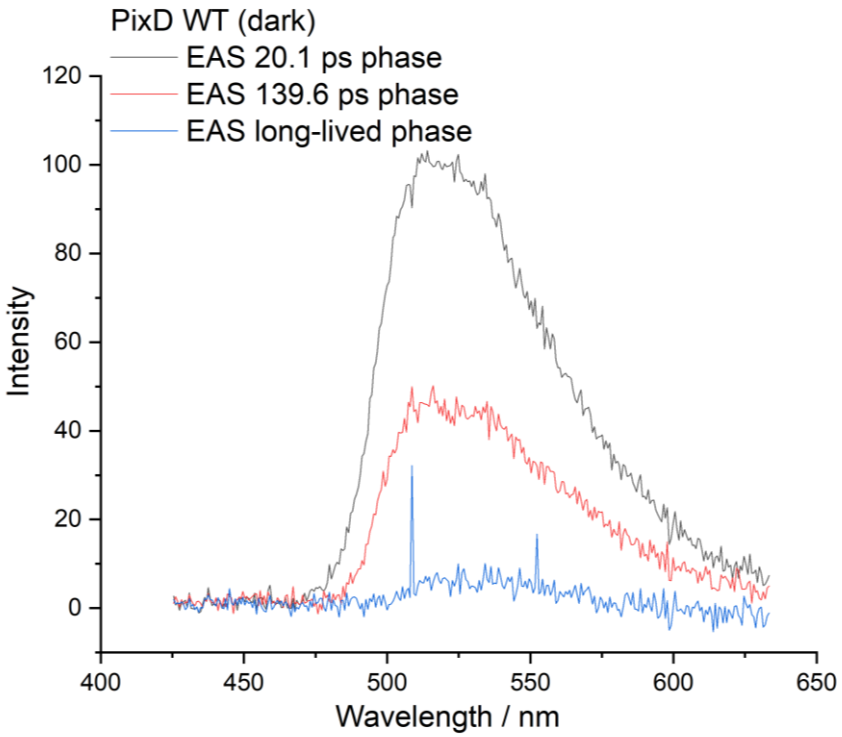


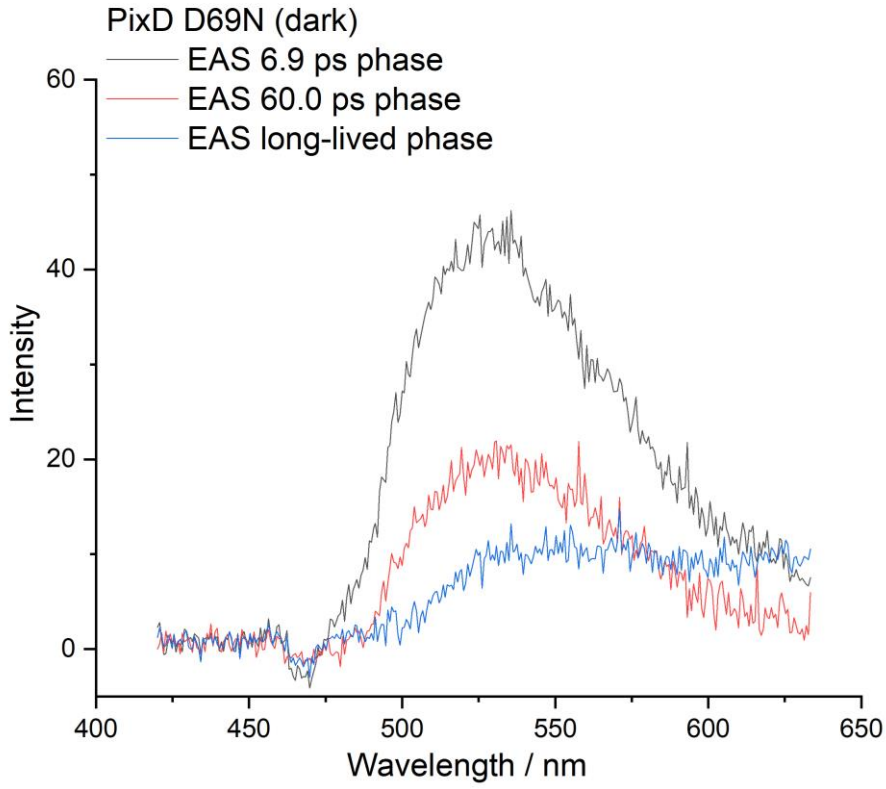


**Figure S2**. A) EAS spectra obtained in the case of WT B) In D67N mutant.

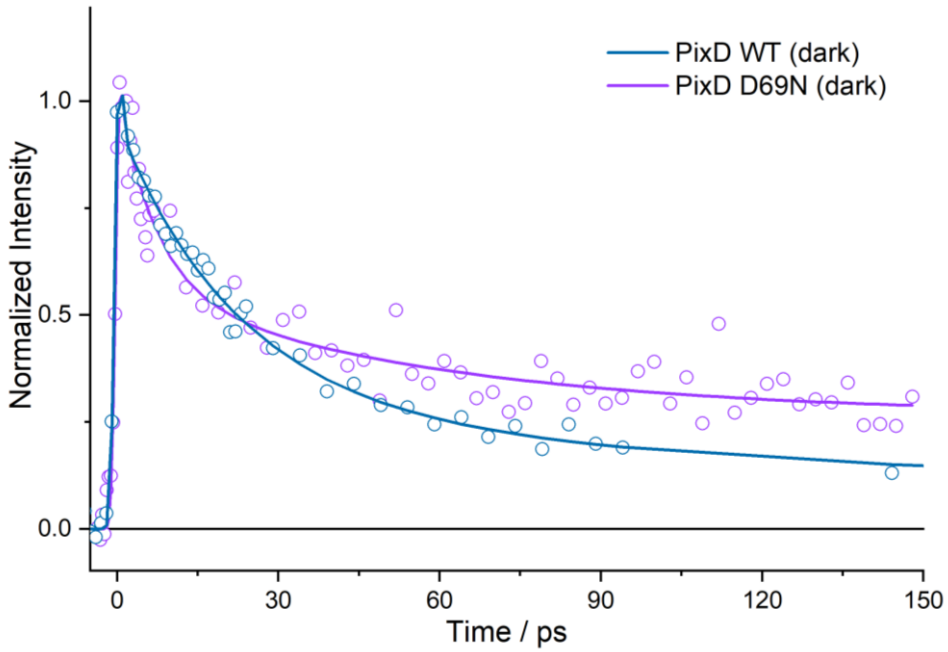


**Figure S3**. Individual kinetics of WT PixD and D69N PixD observed at 520 nm

### 3. Transient absorption measurements on WT and D69N PixD

We performed transient absorption measurements on WT PixD and on PixD D69N mutant and we observed a rather similar behaviour as seen in OaPAC. The back transfer is faster in the mutant than in WT.

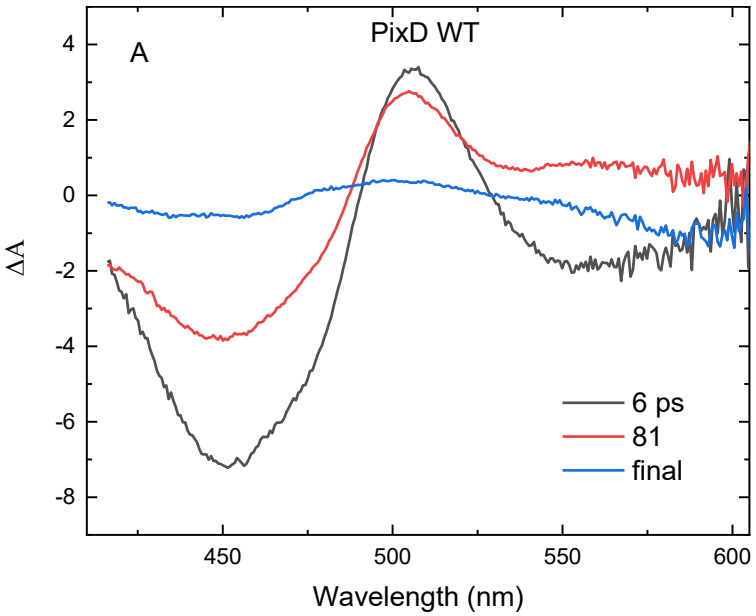


4.

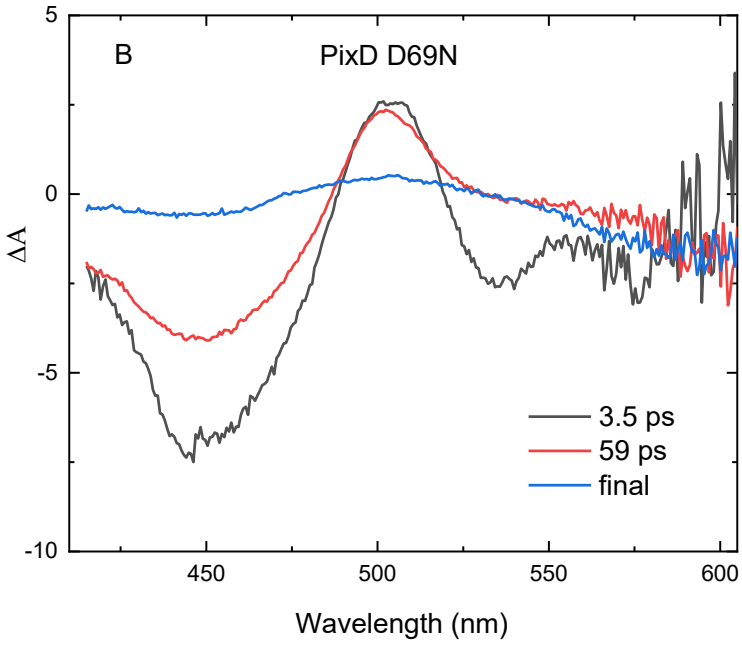


**Figure S4**. EAS spectra after global analysis on A) WT and B) D69N data

5. **Not normalized EAS spectra of WT and D67N OaPAC**

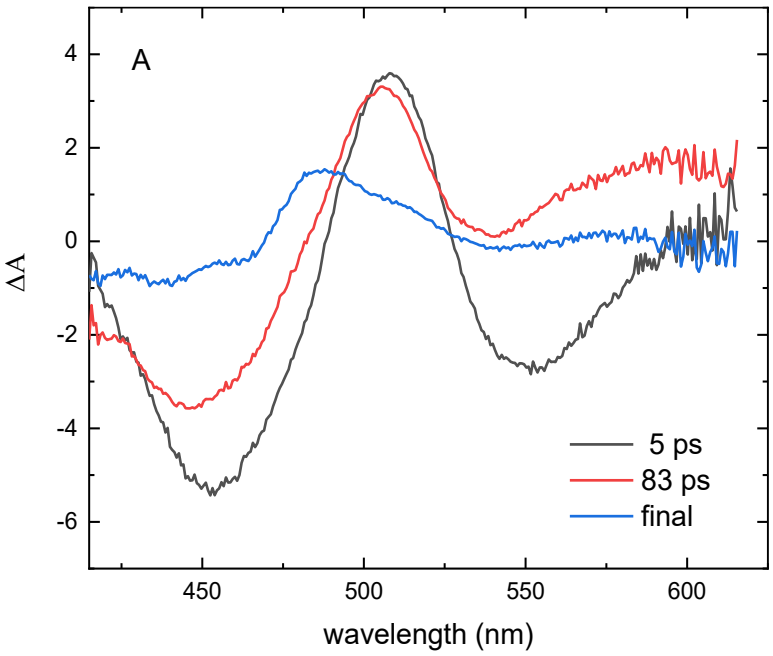


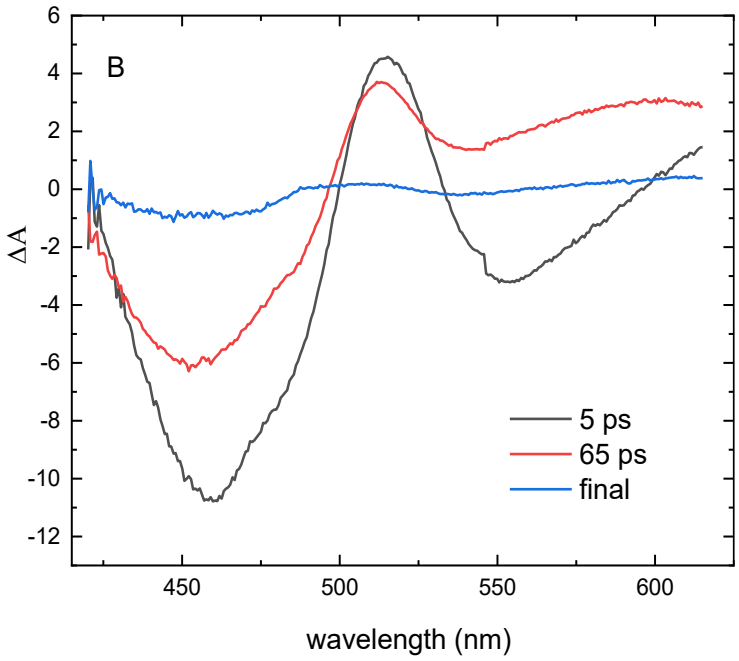


**Figure S5**. Not normalized EAS spectra after global analysis on WT and D67N data. The amplitude of the final state is less than 10 % of the first EAS in the case of D67N measurement

## 6. Kinetics observed by transient absorption in D67N at 600 nm

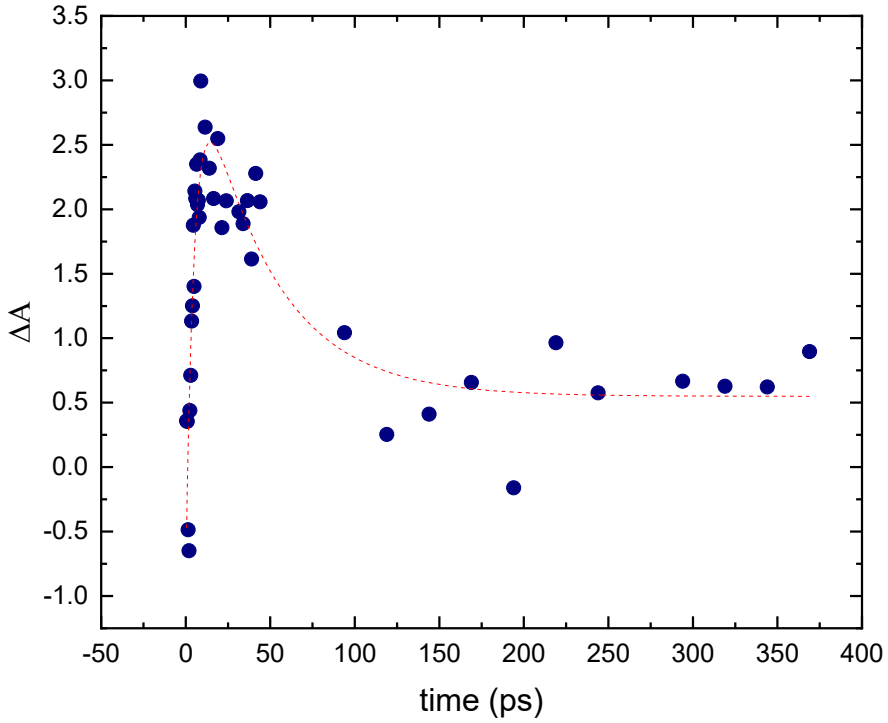


**Figure S6**. Kinetics observed at 600 nm where formation of $FADH^{\bullet}$ should appear. The formation of the neutral radical state and happens with a time constant of 5.1 ± 1.5 ps, relaxation (deprotonation) of this state happens with a time constant 42.5 ± 18 ps. The two time constants overlap with the values of EAS1 and EAS2 determined by the global fit.

## References


1. Liu, B., Liu, H., Zhong, D., andLin, C. (2010) Searching for a photocycle of the cryptochrome photoreceptors Curr Opin Plant Biol **13**, 578-586 10.1016/j.pbi.2010.09.005
2. Liu, Z., Zhang, M., Guo, X., Tan, C., Li, J., Wang, L. *et al.* (2013) Dynamic determination of the functional state in photolyase and the implication for cryptochrome Proceedings of the National Academy of Sciences of the United States of America **110**, 12972-12977 10.1073/pnas.1311077110
3. Solar, S., Gtoff, N., Surdhar, P. S., Armstrong, D. A., andSingh, A. (1991) Oxidation of tryptophan and N-methylindole by N3**.**, Br2**.**- and (SCN)2**.**- radicals in light- and heavy-water solutions: a pulse radiolysis study Journal of Physical Chemistry 3639-3643
4. Goings, J., andHammes-Schiffer, S. (2019) Early Photocycle of Slr1694 Blue-Light Using Flavin Photoreceptor Unraveled through Adiabatic Excited-State Quantum Mechanical/Molecular Mechanical Dynamics Journal of the American Chemical Society **141**, 20470-20479 10.1021/jacs.9b11196